Surface and collective effects in preequilibrium reactions

C. Kalbach
Physics Department, Duke University, Durham, North Carolina 27708-0305
(Received 12 April 2000; published 11 September 2000)

Surface localization of the initial target-projectile interaction has been investigated for incident protons and neutrons at bombarding energies of 14–100 MeV within the framework of the exciton preequilibrium model. Incident neutrons, at least at energies up to around 30 MeV, show a greater amount of surface peaking than do incident protons as judged by the effective well depth available to the hole degree of freedom created. With this difference included, exciton model calculations can describe the energy spectra in all four (N,N) reaction channels with a consistent set of model input. To aid in this study, the excitation of strong spectroscopic collective states was included in the calculations. The addition of giant resonance state excitation has a small but helpful effect. There is a need for additional data, especially for incident neutrons above 26 MeV.

PACS number(s): 24.60.Gv, 24.10.Pa

I. INTRODUCTION

In preequilibrium reaction models the equilibration of a composite nucleus is typically described by the creation of successive particle-hole pairs until the most probable number at equilibrium is approached and the reverse process of pair annihilation begins to compete. These models have been increasingly successful in describing both the energy spectra of particles emitted during the equilibration process and the excitation functions for forming specific product nuclides. This is true both for the phenomenological models such as the exciton [1] and hybrid [2] models and for the more quantum mechanical approaches such as the Feshbach-Kerman-Koonin (FKK) model [3]. As the models have been developed and tested against data, however, one of the thorniest problems has been to account for the relative yields in the four (N,N) channels (where N is a nucleon) using a single, consistent set of input. Until this issue is resolved, a model's predictive value is limited and there are probably areas of relevant physics remaining to be included.

For the hybrid model the problem of simultaneously reproducing the four (N,N) channels was seen in Ref. [2] where the (n,xp) preequilibrium spectra at incident energies around 14 MeV are overestimated while the corresponding (n,xn) spectra are well reproduced and the spectra from (p,xn) reactions at 18–25 MeV are reasonably well accounted for. In the FKK model the problem has often resulted in the need to use different real potential well depths for different channels (see, e.g., Refs. [4,5]). This is true even when the effects of isospin, proton-neutron distinguishability in the state densities, and reasonable changes in optical model potentials are considered as in Ref. [5], or when the potential well depths are compared, as in Ref. [4], based on the projectile energy at the nuclear surface where the proton energies are lowered by the Coulomb barrier.

In the exciton model used in the TUNL phenomenology program the problem became apparent when the input set developed [6,7] using data primarily from proton induced reactions at 18–29 MeV was found [8,9] to underestimate the preequilibrium yield of inelastically scattered neutrons. A discussion in Ref. [8] concluded that there is not sufficient freedom in the exciton model parameters to account for this difference and that excitation of strong collective states is also an unlikely explanation. Instead it was suggested that the initial target-projectile interaction for incident neutrons might occur, on average, closer to the nuclear surface than for incident protons.

Such a difference between neutron and proton projectiles might possibly be explained in terms of the additional Coulomb interaction between the protons and the target, since the nuclear part of the interaction should be similar for the two projectile types, especially for targets with a small neutron excess. Some of the effects of the Coulomb interaction are already included in the proton total reaction cross sections for the entrance channel. These are reduced relative to their neutron counterparts due to Coulomb deflection of some (or, at lower energies, all) of the partial waves away from the nucleus. However, the long range of the Coulomb interaction could also allow a proton projectile to effectively ''reach'' further into the target to excite particle-hole pairs than a neutron projectile could reach. Thus the proton might seem to interact, on average, more toward the interior of the nucleus.

Surface localization of the initial target-projectile interaction in the exciton model was investigated phenomenologically in 1985 (Ref. [10]) using data for proton induced reactions on targets in the nickel region. Sample energy spectra were analyzed to determine the average effective potential well depth available to the hole degree of freedom produced in the interaction. The resulting values expressed as a function of incident energy were found to work adequately in other mass regions and have been assumed to apply for neutron projectiles as well. Given the observations of Ref. [8], the issue of surface localization has been revisited using data for both projectile types, and the results are presented here.

To facilitate this work, a model due to Kalka *et al.* [11] for the excitation of strong, low-lying collective states in inelastic scattering was included in the exciton model code system PRECO-E (Ref. [12]) as described in the next section. The study of surface effects is set forth in Sec. III, and the role of giant resonance states is considered in Sec. IV. A comparison of calculations with the entire project data base is contained in Sec. V. The last section summarizes the results, discusses the need for additional data, and notes open

questions for study at higher incident energies.

II. EXCITATION OF COLLECTIVE STATES

In models like the exciton model which take a single particle view of the states of a nucleus, it is clear that strong collective states are not considered. Yet it is also clear that such states frequently represent a prominent feature in the energy spectra of inelastically scattered particles. To account for these peaks, another model is needed, and this work uses the model of Ref. [11]. The same authors have also proposed more quantum mechanical descriptions, but the model of Ref. [11] is developed along lines more suited to the simple, phenomenological nature of the exciton model.

A. Model

The cross section given in Ref. [11] for exciting a collective state of multipolarity λ is expressed in terms of the wave numbers k_i and k_f and penetrabilities P_i and P_f for the incoming and outgoing particles (denoted by the subscripts i and f). It is given by

$$\frac{d\sigma_\lambda(k_i,k_f)}{d\varepsilon_f}=\left(\frac{m\mathcal{V}}{2\pi\hbar^2}\right)^2\frac{1}{(k_iR)^2}\frac{k_f}{k_i}\frac{\beta_\lambda^2}{2\lambda+1}\times V_R^2P_iP_f\,\delta(E_\lambda-\varepsilon_i+\varepsilon_f), \quad (1)$$

where E_λ and β_λ are the excitation energy and deformation parameter of the collective state, and ε_i and ε_f are the center-of-mass kinetic energies of the particles. The quantity m is the particle mass, $\mathcal{V}$ is the nuclear volume, R is its radius, and V_R is the real optical model potential. The penetrability factors were approximated by 1 for neutrons and σ_p/σ_n for protons where the σ's are total reaction cross sections evaluated at the appropriate energy. The delta function places the cross section at the energy of the collective state. In practice it is replaced by a Gaussian $\mathcal{P}(E_\lambda,s)$ of adjustable width s centered at E_λ. The width of the Gaussian accounts for the experimental energy resolution and any inherent spreading of the collective strength.

In the present work, Eq. (1) is reformulated in terms of the energies of the particles, and the transmission factors are taken to be ratios of the total reaction cross sections to the corresponding geometric cross sections. With these changes and the inclusion of the Gaussian smoothing function the formula becomes

$$\frac{d\sigma_\lambda(\varepsilon_i,\varepsilon_f)}{d\varepsilon_f}=\frac{2m}{9\hbar^2}\frac{\varepsilon_f^{1/2}}{\varepsilon_i^{3/2}}\frac{\beta_\lambda^2}{2\lambda+1}V_R^2R^4\times\frac{\sigma_i(\varepsilon_i)}{\sigma_{\mathrm{geom},i}(\varepsilon_i)}\frac{\sigma_f(\varepsilon_f)}{\sigma_{\mathrm{geom},f}(\varepsilon_f)}\mathcal{P}(E_\lambda,s). \quad (2)$$

Values of $V_R=50$ MeV and $R=1.23\times A^{1/3}$ fm are used. To conserve cross section, the amount due to collective state excitation is subtracted from the entrance channel reaction cross section in determining how much goes into the exciton model calculations.

The collective state model of Ref. [11] gives only angle integrated cross sections. Most of the spectra analyzed in this work are angle integrated, but for spectra at a fixed angle it is assumed that the collective state angular distributions follow the global empirical systematics [13] used in the rest of the calculations. This is not correct in detail since the angular distributions typically show structure characteristic of the specific l transfer involved. However, sample comparisons for reactions at 14 and 61 MeV show that the systematics are a reasonable approximation to the average trend of the data, especially at 30° and above. Nor were collective states subtracted from the data used to develop the systematics.

B. Collective state parameters

Which collective states should be included? Kalka's early work [14] includes the low-lying $2+$, $3-$, and $4+$ levels. In Ref. [11] and later papers only the $2+$ and $3-$ levels are considered, and this choice has generally been adopted in preequilibrium work. Occasionally (see Ref. [5]) a whole host of known levels, including broad giant resonance states, have been included, accounting for up to half of the total preequilibrium strength in the inelastic channel. The present work begins by considering only the strong $2+$, $3-$, and $4+$ collective states since these represent a dramatic relocalization of strength and are typically clearly visible in the spectrum.

The issue of when to calculate $4+$ collective strength was resolved empirically. For even-even targets, the $4+$ strength is included when those states appear in the inelastic scattering spectra above the general trend of the data. For nuclides for which data are unavailable or ambiguous and for odd-A targets, guidance from neighboring nuclei is used. For the heavier ($A>130$) deformed nuclei where the energies of the lowest $4+$ levels are less than 0.5 MeV, the $4+$ states have not been included because of their proximity to the elastic peak and because they are generally rotational levels that would be excited mainly by double $E2$ transitions. For nuclei in the vicinity of the tin and lead shell closures, the $4+$ levels are close to the $3-$ and $2+$ levels, respectively, making it necessary to subtract the intensity of the lower λ level in making an assessment.

The values for E_λ and β_λ are most important for lighter and near-shell nuclides where the collective states lie higher in excitation energy. For even-even targets, starting values for E_λ and β_λ have been taken from the tabulations of Ref. [15] for the lowest $2+$ levels and of Ref. [16] for the lowest $3-$ levels. The energies of the lowest $4+$ levels were taken either from the Table of Isotopes [17] or from the Lawrence Berkeley National Laboratory web site using the program Isotope Explorer. Values for β_4 were assumed to be between zero and min (β_2,β_3). Often a value of $0.75\min(\beta_2,\beta_3)$ is appropriate.

If the data for a specific nuclide show a higher level of the same spin and parity carrying the bulk of the collective strength for a given multipolarity, the higher level was substituted and β_λ was adjusted empirically. This occurs for the $3-$ strength in ^{54}Fe and the $4+$ strength in ^{52}Cr, ^{54}Fe, and

TABLE I. Summary of the collective state parameters used in model calculations. The energies are given in MeV.

Target	$E(2+)$	$E(3-)$	$E(4+)$	β_2	β_3	β_4
^{24}Mg	1.37	7.62	4.12	0.61	0.27	0.27
^{27}Al	1.0 2.2 } 2.32 3.0	7.2	4.47	0.19 0.27 } 0.44 0.29	0.22	0.16
^{28}Si	1.78	6.88	4.62	0.41	0.28	0.21
^{40}Ca	3.90	3.74		0.12	0.34	
^{48}Ca	3.83	4.51		0.10	0.20	
^{46}Ti	0.89	3.06	2.01	0.32	0.14	0.10
^{48}Ti	0.98	3.36	2.30	0.27	0.19	0.15
^{51}V	1.49	3.90	2.52	0.20	0.16	0.12
^{50}Cr	0.78	4.05	1.88	0.29	0.15	0.11
^{52,53}Cr	1.43	4.56	2.77	0.22	0.15	0.11
^{55}Mn	0.84	4.32	2.3	0.24	0.18	0.18
^{54}Fe	1.41	6.34	3.83	0.20	0.15	0.11
^{56}Fe	0.85	4.51	3.12	0.24	0.18	0.13
^{58}Fe	0.81	3.84	3.1	0.26	0.13	0.09
^{59}Co	1.33	3.84		0.21	0.19	
^{58}Ni	1.45	4.48	2.46	0.183	0.18	0.09
			3.62			0.09
^{60}Ni	1.33	4.04	4.96	0.207	0.19	0.19
^{62}Ni	1.17	3.76	2.34	0.198	0.225	0.198
^{63}Cu	1.17	3.76	2.34	0.20	0.18	0.11
^{65}Cu	1.35	3.56	2.61	0.18	0.18	0.11
^{64}Zn	0.99	3.00	2.31	0.23	0.23	0.11
^{70}Ge	1.04	2.56	2.15	0.224	0.24	0.11
^{89}Y	2.01	2.74	3.69	0.104	0.17	0.10
^{90}Zr	2.19	2.75	4.33	0.091	0.16	0.11
^{91}Zr	2.19	2.75	4.33	0.091	0.16	0.11
^{92}Zr	0.934	2.34	1.50	0.103	0.17	0.10
^{94}Zr	0.918	2.06	1.47	0.09	0.19	0.09
^{93}Nb	0.903	2.44	1.54	0.13	0.17	0.13
^{92}Mo	1.51	2.85		0.106	0.17	
^{94}Mo	0.871	2.53		0.161	0.163	
^{95}Mo	0.825	2.38		0.166	0.17	
^{96}Mo	0.778	2.24		0.172	0.18	
^{97}Mo	0.782	2.13		0.170	0.19	
^{98}Mo	0.787	2.02		0.168	0.198	
^{100}Mo	0.536	1.91		0.231	0.18	
^{103}Rh	0.516	2.12		0.23	0.135	
^{104}Pd	0.556	2.19		0.21	0.13	
^{105}Pd	0.534	2.14		0.22	0.15	
^{106}Pd	0.512	2.08		0.23	0.17	
^{108}Pd	0.434	2.05		0.24	0.15	
^{110}Pd	0.374	2.04		0.26	0.134	
^{107}Ag	0.573	2.14		0.20	0.19	
^{109}Ag	0.546	2.06		0.21	0.16	
^{115}In	1.29	2.27		0.112	0.18	
^{116}Sn	1.29	2.27	2.39	0.112	0.18	0.11
^{117}Sn	1.26	2.30	2.34	0.112	0.18	0.11
^{118}Sn	1.23	2.32	2.28	0.111	0.171	0.11
^{119}Sn	1.20	2.36	2.24	0.110	0.16	0.11
^{120}Sn	1.17	2.40	2.19	0.108	0.16	0.11
^{122}Sn	1.14	2.49	2.14	0.104	0.150	0.10

TABLE I. (*Continued*).

Target	$E(2+)$	$E(3-)$	$E(4+)$	β_2	β_3	β_4
^{124}Sn	1.13	2.61	2.10	0.095	0.13	0.095
^{121}Sb	1.17	2.40	2.19	0.108	0.16	0.108
^{123}Sb	1.14	2.49	2.14	0.104	0.150	0.10
^{159}Tb	0.083	1.16		0.34	0.090	
^{165}Ho	0.077	1.28		0.345	0.060	
^{169}Tm	0.112	1.41		0.32	0.057	
^{181}Ta	0.097	1.37		0.26	0.050	
^{182}W	0.100	1.37		0.249	0.050	
^{183}W	0.106	1.30		0.24	0.050	
^{184}W	0.111	1.22		0.24	0.051	
^{186}W	0.123	1.04		0.224	0.05	
^{197}Au	0.384	1.69	0.962	0.119	0.051	0.05
^{204}Pb	0.899	2.62	1.27	0.041	0.09	0.041
^{206}Pb	0.803	2.65	1.68	0.032	0.10	0.032
^{207,208}Pb, ^{209}Bi	4.08	2.62	4.32	0.054	0.11	0.054
		5.52			0.05	

^{56}Fe. For ^{208}Pb, there seems to be additional collective strength at around 5.5 MeV in the (n,xn) data of Takahashi [18]. Since there are several closely spaced $3-$ levels in this vicinity, the strength has been included in the calculations as an additional $3-$ collective level with about half the β_3 of the lowest $3-$ level. In ^{58}Ni there appear to be two strong $4+$ levels, and both have been included.

For odd-A targets, E_λ and β_λ were generally taken as the average between the values for the neighboring even-even targets. However, for nuclei one unit away from a shell closure, the closed shell values are used based on the similarity between the measured ^{208}Pb and ^{209}Bi(n,xn) spectra at 14.1 MeV. For ^{27}Al, the $2+$ strength is believed to be divided among three levels at about 1.0, 2.2, and 3.0 MeV, with a centroid at 2.32 MeV, half an MeV above the nominal value. The β_2 values for these states have been adjusted so that the corresponding $B(E2)\uparrow$ values sum up to the average for ^{26}Mg and ^{28}Si. For ^{27}Al, ^{51}V, and ^{59}Co the $3-$ strength is shifted by about $+0.3$, -0.6, and -0.2 MeV, respectively. The β_3 values were not altered. Finally, the β_3 values for ^{63}Cu and ^{65}Cu were each reduced by a factor of about 0.8 based on the 14 MeV neutron scattering data on natural copper.

A summary of the collective state parameters used in this work is shown in Table I.

What about giant resonance states? Since their contribution to angle integrated spectra is not expected to be large, this subject is deferred to Sec. IV.

III. SURFACE LOCALIZATION OF THE INITIAL INTERACTION

In the exciton model, the effects of surface localization of the initial target-projectile interaction are seen because the shallower potential well depth in the surface region limits the amount of excitation energy that the newly formed hole degree of freedom can carry. This forces more of the available energy to be carried by the particle degrees of freedom, leading to more high energy particle emission than in the absence of surface effects. Particle-hole state densities in the exciton model are typically derived for an infinitely deep well, and finite well depth (FWD) corrections are then applied. When surface localization occurs, a shallower average effective potential well depth $V_{\rm eff}$ is used for calculating the FWD corrections for states with one hole degree of freedom, while the central well depth of 38 MeV is used for more complex configurations. As discussed in Ref. [10], the FWD correction is actually calculated for a range of well depths centered around $V_{\rm eff}$ and a weighted average is taken. The width of the averaging distribution is greatest for $V_{\rm eff}$ about half way between the physical limits of 0 and 38 MeV and is zero at the physical limits. The well depths are given relative to the Fermi level.

A. Method

In this work as in Ref. [10] surface effects are studied phenomenologically. A sample data set was selected consisting of measured inclusive energy spectra (angle integrated if available) for 58 reaction/energy pairs covering a range of targets, all four (N,xN) reaction channels, and bombarding energies up to 100 MeV. Model calculations were first performed assuming no surface localization ($V_{\rm eff}=38$ MeV). All other aspects of the calculations were as in Ref. [9]. Some assumption had to be made about isospin conservation during the preequilibrium phase of the reaction for incident energies of 35–65 MeV. The results proved fairly insensitive to this choice, so isospin is assumed to be conserved up to 45 MeV as at lower energies but mixed above 60 MeV in agreement with preliminary work at 90 MeV. The calculations were then repeated varying $V_{\rm eff}$. Figure 1 shows the sensitivity of two sample spectra [19,20] to changes in $V_{\rm eff}$. At the lower bombarding energies and particularly for the lighter targets, the evaporation component extends over much of the spectrum, thus reducing sensitivity to surface effects. As the incident energy or target mass increases, the

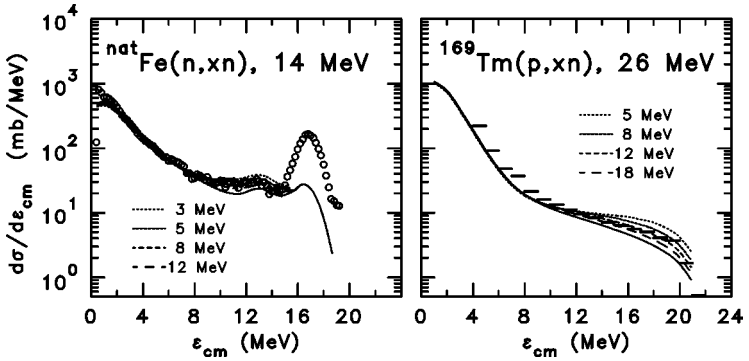

FIG. 1. Sensitivity of the reaction calculations to changes in the average effective potential well depth felt during the initial target-projectile interaction. The points show the data, and the curves give the calculated results for the indicated values of $V_{\rm eff}$. The solid curves are for no surface effects and use the central well depth of 38 MeV.

sensitivity first increases but then levels off as preequilibrium emission from more complex configurations and, eventually, secondary preequilibrium emission become more important.

For each spectrum studied, two ranges of $V_{\rm eff}$ were tabulated: a narrower range that gives good agreement with experiment and a broader range that gives acceptable agreement. Agreement in overall spectral shape was preferred over agreement in intensity in the sensitive region of the spectrum since the data could be affected by a normalization error or the calculations could be using less-than-optimal values for other model parameters. The selected ranges are somewhat subjective, so their limits vary slightly as the process is repeated, but the overall trends remain the same.

B. Results

For each projectile type (n and p) the average effective potential well depths were grouped by target mass, incident energy, and reaction channel, looking for trends. From the results shown in Figs. 2 and 3, the following preliminary observations can be made.

(i) All of the data which are sensitive to $V_{\rm eff}$ yield values much smaller than the central well depth of 38 MeV, implying that surface localization is important for both projectiles.

(ii) There is no discernible systematic dependence on target mass.

(iii) The $V_{\rm eff}$ values for incident neutrons are less than the corresponding values for incident protons at incident energies up to 26 MeV, supporting the hypothesis that surface localization is more important for neutron projectiles.

(iv) The question of a systematic difference between the inelastic and exchange channels is unclear. Incident neutrons at 14 MeV show no systematic difference. For incident protons, inelastic scattering tends to yield shallower $V_{\rm eff}$ than do exchange reactions, though often a single value will adequately account for both.

Given the lack of a discernible A dependence, a single $V_{\rm eff}$ (with approximate uncertainties) was selected that seemed to give the best overall accounting of the data for each (N,xN) reaction type and incident energy bin. Another value balancing the effects of the inelastic and exchange channels for each projectile was also selected. These ''average'' values are given in Table II.

While a systematic difference may exist between $V_{\rm eff}$ values for the inelastic and exchange channels, there is no obvious reason to expect one. Further, given the long-range Coulomb component of the p-p interaction, it would be strange for incident protons to excite target protons close to the nuclear surface and neutrons further inside. One possible explanation for an apparent inelastic/exchange channel difference is background in the inelastic proton spectra due to tails of the elastic scattering peak when passive collimators

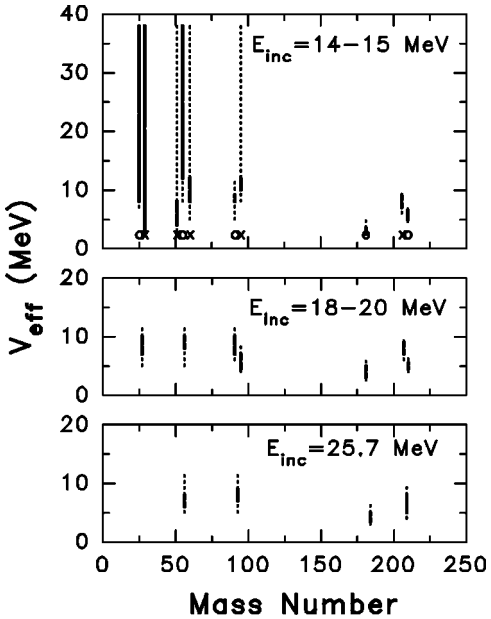

FIG. 2. Summary of $V_{\rm eff}$ for incident neutrons, plotted versus target mass for the indicated ranges of incident energy. The heavier, solid vertical bars denote the values giving the best agreement with the data while the lighter, dashed bars show the range giving acceptable agreement. The bars have been shifted slightly on the mass scale for display purposes. An ''×'' below a bar indicates results for exchange reactions, while an ''○'' indicates inelastic scattering. For incident energies above 15 MeV, all of the results are for inelastic scattering.

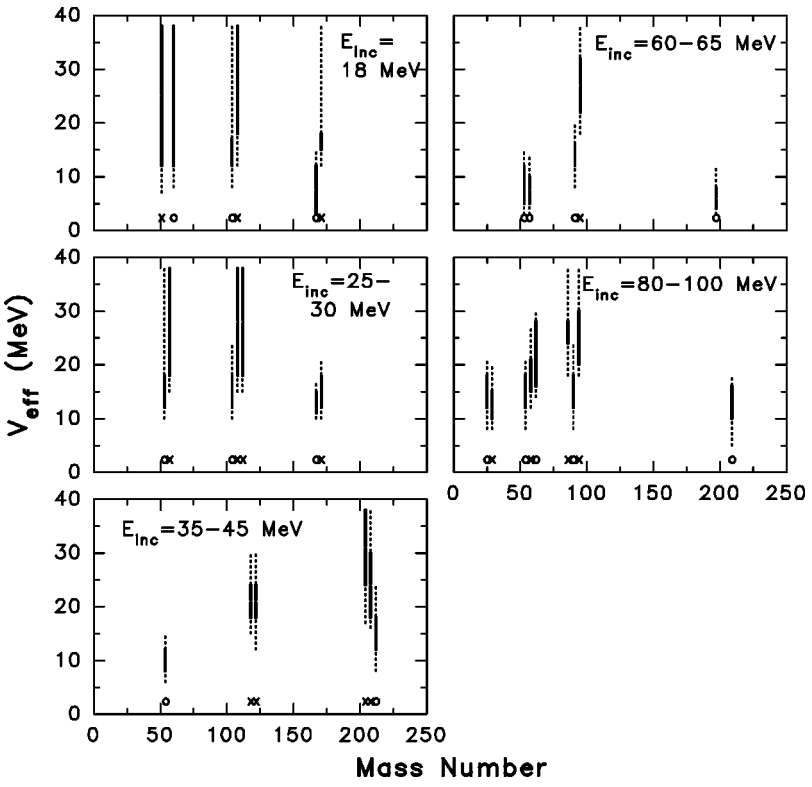

FIG. 3. Summary of $V_{\rm eff}$ values for incident protons. The display is analogous to that in Fig. 2.

are used. Another is contributions to the inelastic data from giant resonance (GR) states which are not yet included in the calculations. For both proton and neutron projectiles, the shallowest $V_{\rm eff}$ tend to occur for inelastic scattering on the heavy deformed nuclei ^{169}Tm, ^{181}Ta, and ^{184}W for which the GR contributions should be most evident. (These values accordingly received less weight than the others in constructing the results in Table II.) Finally, the observed inelastic/exchange difference is greatest between 35 and 65 MeV where data are quite limited, while at both lower and higher energies, values of $V_{\rm eff}$ exist which adequately account for the data from both channels. For these reasons, it has been provisionally assumed that surface effects in the inelastic and exchange channels are the same. The question of GR contributions is addressed in the next section.

The overall average values from Table II are plotted as a function of incident energy in Fig. 4 where the difference between neutron and proton projectiles is quite clear. The proton data suggest $V_{{\rm eff},p}=17$ MeV, independent of bombarding energy. The neutron results also appear to be independent of energy up to 26 MeV but with $V_{{\rm eff},n}=7$ MeV. Above 26 MeV only a 60-MeV ^{58}Ni(n,xp) spectrum has been analyzed. Thus the trend indicated by the point at that energy is highly tentative. Nevertheless, the full set of neutron results have been fit with the somewhat arbitrary functional form

$$V_{{\rm eff},n}=20\ {\rm MeV}-13\ {\rm MeV}\left[1+\exp\left(\frac{E_{\rm L}-45\ {\rm MeV}}{4\ {\rm MeV}}\right)\right]^{-1}, \tag{3}$$

where $E_{\rm L}$ is the laboratory energy of the projectile. This produces the dashed line in Fig. 4. Clearly incident neutron data above 26 MeV are badly needed.

The present proton results differ somewhat from those

TABLE II. Summary of the average effective potential well depths giving the best overall description of data for different incident energies. All values are in MeV.

$E_{\rm inc}$	(n,xn)	(n,xp)	(n,xN)	(p,xp)	(p,xn)	(p,xN)
14–15	7.5±3	8±1	7±3	⩾18		18^{+20}_{-3}
18–20	7±2		7±2	13^{+3}_{-5}	18±6	16±3
25–30	7±1		6.5±1	15^{+2}_{-5}	18±3	17.5±2
35–45				12^{+3}_{-4}	24±6	17±4
60–65		(19±5)	(20±3)	10^{+4}_{-2}	27±10	14±5
80–100				16±2	19±2	17.5±3

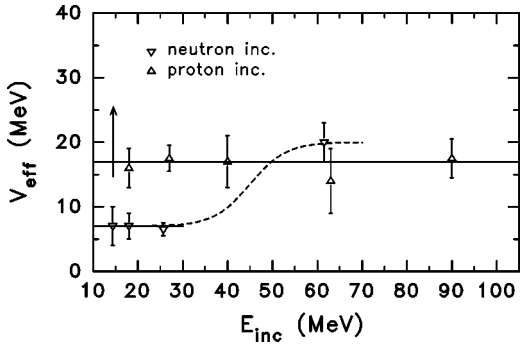

FIG. 4. Incident energy dependence of $V_{\rm eff}$ for neutron and proton projectiles. The lines show the adopted energy dependence.

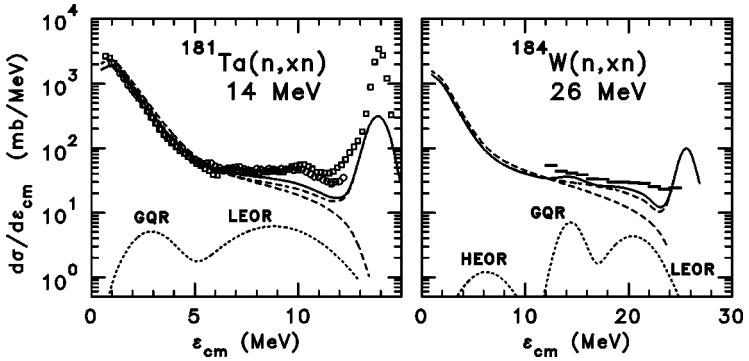

FIG. 5. Effect of revised surface localization and the inclusion of collective state excitation in model calculations. The points and bars show the data [19,28,29]. The lower dashed curves show the previous calculations [9], while the upper dashed curves show the calculated curves with the revised $V_{\rm eff}$ and the excitation of spectroscopic collective states. The solid curves also include the giant resonance contributions which are shown separately as dotted curves.

obtained in Ref. [10] where surface localization was assumed to diminish below about 40 MeV. This was suggested mainly by the lowest energy spectrum at 26 MeV, which was fairly insensitive to $V_{\rm eff}$. The current results utilizing a more robust version of the exciton model and a more comprehensive data base should be more reliable.

C. Perspectives

In the present work, a single $V_{\rm eff}$ value is used for each reaction studied, independent of emission angle. This is supported by recent semiclassical distorted wave (SCDW) model calculations [21] of (p,xp) and (p,xn) reactions on several nuclei at incident energies of 62–160 MeV. Figure 9 of that paper considers the ^{90}Zr(p,xp) reaction at 120 MeV (emission energies of 40 and 100 MeV) and shows the angular spread of contributions to direct emission from *N*-*N* scatterings occurring at different radii. The figure shows a quasifree scattering peak originating at $r>6$ fm occupying a relatively narrow angle range, but otherwise the emission is dominated by the bins with radii of 2–4 fm and, especially, 4–6 fm at all angles for which significant emission occurs.

Looking in more detail, the much smaller contribution from radii of 0–2 fm suggests that much of the contribution from the 2–4 fm bin comes from the larger radii. Thus direct emission seems to occur mainly following interactions at radii of 3–6 fm where the nuclear density goes from 0.96 to 0.10 of its central value. This is roughly consistent with $V_{{\rm eff},p}$ in this work which is found to be about half the central well depth.

Suggestive but certainly not definitive evidence in support of a difference between the amount of surface localization for incident protons and neutrons can be found by comparing the proton results of Ref. [21] with the primarily neutron results of Ref. [22], another paper looking at surface localization using a semiclassical approach. The difficulty is that these papers calculate and display slightly different quantities and consider different incident energies. Avrigeanu *et al.* [22] show the probability for absorption of neutrons from the entrance channel as a function of distance from the center of a ^{93}Nb nucleus for incident energies of 10–50 MeV. The peak of the absorption, and thus the most probable ''location'' of the initial interaction, occurs at 6.1 to 6.5 fm, with the smaller values at the higher energies. The full width at half maximum (FWHM) of the distributions is about 2.6 fm. These results include two types of strength that are not included in the 3–6-fm estimate made for incident protons: the strength ultimately going into quasifree scattering (probably more concentrated at the larger radii) and the strength that would undergo additional particle-hole pair creation interactions rather than direct particle emission (and might be more concentrated toward smaller radii). These two contributions are likely to be somewhat offsetting. The shift of the peak position with incident energy in Ref. [22], if extrapolated to 120 MeV, would tend to push it more toward the radii found in Ref. [21], but the shift is most rapid at 10–20 MeV where the imaginary optical potential is changing most rapidly from a surface dominated to a volume dominated form. At 50 MeV and above the imaginary potential has essentially a purely volume form, so that the changes should be smaller.

Thus these two references support the result of strong surface localization of the initial interaction for both proton and neutron projectiles and are suggestive of more such localization for incident neutrons. Future, more consistent SCDW calculations run for the two projectiles at similar energies should hopefully take account of the longer range of the Coulomb part of the proton-target interaction and should involve several targets with different neutron excesses so as to see how much of any observed effect might be due to the symmetry terms in the optical model potential. The present work does not show a dependence on *A* or, by inference, on $(N-Z)/A$.

It should also be reiterated that the current choices for $V_{\rm eff}$ are *effective* values. The work of Ref. [10] showed that if long-range deviations from the equispacing model for the single particle states are taken into account, the values can change somewhat (by 1–2 MeV if an $e^{1/2}$ dependence is assumed). Similarly other aspects of the calculations could affect the values arrived at. However, the general conclusions that surface effects are important, and that they are more important for incident neutrons than protons should remain valid, as should the trends of $V_{\rm eff}$ with *A* and incident energy.

IV. ROLE OF GIANT RESONANCE STATES

In order to test the present results and to better assess the need to include the GR states, a set of model calculations was run for the full data base used in Refs. [8,9] plus the extra spectra employed in the previous section, again using the input parameters of Ref. [9] but with the revised $V_{\rm eff}$ values. The input is described in Sec. V. The results for incident neutrons are often improved relative to earlier studies, especially for the (n,xn) spectra. For incident protons, the agreement tends to be similar to that seen in earlier work or somewhat better. Comparisons for both projectile types indicate that more inelastic cross section would be helpful at the higher emission energies where GR states should contribute. This is especially noticeable for heavy deformed targets.

Given the general apparent need for additional inelastic strength in the GR region of the spectrum, such strength was included in the calculations using the model employed for the discrete collective states and GR parameters from two reviews [23,24]. The resonance energy is given a smooth A dependence, its β_l is determined from the fraction of the energy weighted sum rule (EWSR) which is assumed to be used, and its width is taken from empirical trends. The four lowest energy isoscalar GR's are considered.

The lowest in energy is the low energy octopole resonance or LEOR which consists of $1\hbar\omega$ $3-$ transitions. It has been included in preequilibrium reaction calculations by other groups [5,25,26], though with widely varying intensities. In the present work, its excitation energy is taken to be $E_{\rm LEOR}=31A^{-1/3}$ MeV and its β_3 is chosen so that the LEOR plus the spectroscopic $3-$ collective state(s) will exhaust 30% of the $l=3$ EWSR. The remaining 70% is reserved for the high energy octopole resonance. For $l\geqslant 2$, the sum rule for a uniform mass distribution with radius $R=1.23A^{1/3}$ fm is [27]

$$S_l=\sum_i E_{l,i}\cdot\beta_{l,i}^2=\frac{2\pi\hbar^2}{3AmR^2}l(2l+1)$$
$$=57.5A^{-5/3}l(2l+1)\ \ \text{MeV}, \qquad (4)$$

where m is the nucleon mass. This gives $S_3=1208A^{-5/3}$ MeV. The LEOR width is taken as $\Gamma_{\rm LEOR}=5$ MeV corresponding to a Gaussian width parameter of $s_{\rm LEOR}=2.1$ MeV.

Next lowest in energy is the giant quadrupole resonance or GQR. It is taken to have $E_{\rm GQR}=65A^{-1/3}$ MeV and a width of $\Gamma_{\rm GQR}=85A^{-2/3}$ MeV (or $s_{\rm GQR}=36A^{-2/3}$ MeV), which is the author's fit to the values shown in Ref. [23]. The GQR plus the spectroscopic $2+$ collective state are assumed to exhaust the EWSR of $S_2=575A^{-5/3}$ MeV.

The energy of the giant monopole resonance (GMR) is sometimes fit with an $A^{-1/3}$ dependence with or without a second term in $A^{-1/6}$, but the values given in Ref. [24] are more suggestive of a linear dependence which has here been taken to be $E_{\rm GMR}=(18.7-0.025A)$ MeV. Its width is about $\Gamma_{\rm GMR}=3$ MeV. The monopole EWSR for a uniform mass distribution is given by [27]

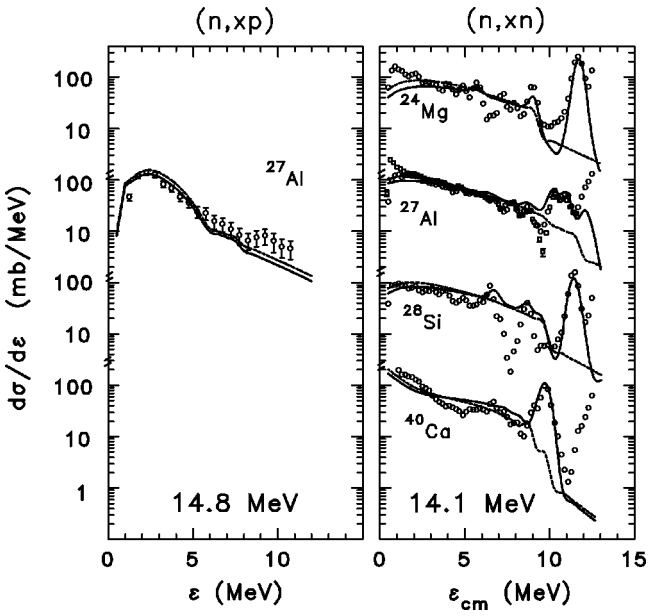

FIG. 6. Comparison between calculation and experiment for reactions on light targets at incident energies of 14–15 MeV. The data are shown as points and are taken from Refs. [18,19,32,33]. The dashed curves show the calculated results from Ref. [9], while the solid curves give the results from the current work. For the (n,xp) reactions, the data are in the laboratory system while the calculated curves are plotted vs the channel energy.

$$S_0=\sum_i E_{0i}\cdot\beta_{0i}^2=\frac{5\hbar^2}{6AmR^2}=23A^{-5/3}\ \ \text{MeV} \qquad (5)$$

so that the GMR is weak compared to the higher l GR states, and it has been ignored in the calculations.

Finally the high energy octopole resonance (HEOR) contains the $3\hbar\omega$ $3-$ transitions and has an average energy of about $E_{\rm HEOR}=115A^{-1/3}$ MeV. Its β_3 is determined assuming that this state exhausts the remaining 70% of the $l=3$ EWSR. It's width is assumed to be $\Gamma_{\rm HEOR}=(9.3-A/48)$ MeV ($s_{\rm HEOR}=(4.0-A/113)$ MeV), the author's fit to the values shown in Ref. [23].

The effects of including the giant resonance states on sample inelastic scattering spectra for heavy deformed targets is shown in Fig. 5 along with the measured spectra [19,28,29]. While the contributions from individual GR's can be seen in the calculations, their effect is relatively small and inadequate to resolve all discrepancies with experiment. Thus while it is helpful and instructive to include these states, they do not play a major role in determining the preequilibrium energy spectrum.

V. COMPARISONS WITH FULL DATA BASE

As a final test of the exciton model with the modified surface effects and the inclusion of both spectroscopic and giant resonance collective excitations, a new set of calculations was run using the code PRECO-E and the current global input set. The data base considered is the full set from Refs. [8,9] (about 150 spectra at 14–29 MeV and 8 spectra at

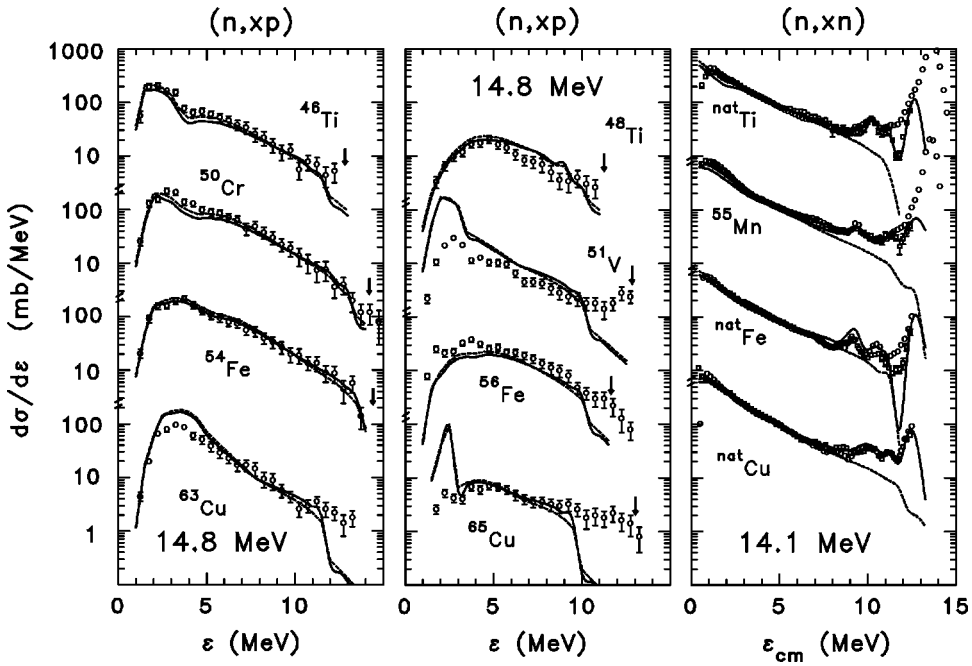

FIG. 7. Comparison between calculation and experiment for reactions on targets with $A=45-65$ at incident energies of 14–15 MeV. The points and curves have the same significance as in Fig. 6. The vertical arrows show the location of the ground state transitions for the exchange reactions. The data are from Refs. [18,19,32–36].

90 MeV) plus the 13 extra systems at 35–100 MeV used in studying surface localization. The model assumptions and input set are taken from Ref. [9] but with the modified $V_{\rm eff}$ values and the additional collective state parameters described above. Since the global input set has evolved gradually over a series of papers, it is summarized here.

A. Model input

The calculations start with the projectile nucleon as a particle degree of freedom and with no hole degrees of freedom. Proton and neutron degrees of freedom are treated distinguishably and are assumed to be created or destroyed in particle-hole pairs by the residual interactions. The calculations are done in closed form using the never-come-back approximation but with the possibility of an exciton scattering interaction (changing a proton pair into a neutron pair or vice versa) prior to particle emission or creation of the next particle-hole pair. The equispacing model state densities occurring in the rate expressions for both particle emission and the residual interactions are modified for the effects of pairing, shell structure, isospin, and the finite potential well depth. Isospin is assumed to be conserved during the preequilibrium phase of the reaction at incident energies up to 45 MeV, and mixed otherwise. The pairing energies, shell gaps and isospin symmetry energies are taken from independent sources and are given in Ref. [6]. The FWD corrections use the central well depth of 38 MeV except for states with one hole degree of freedom where $V_{\rm eff}$ is used.

As in Ref. [6], the main exciton model parameters are the equispacing model single particle state densities for protons and neutrons, $g_{\pi 0}=Z/15$ MeV^{-1} and $g_{\nu 0}=N/15$ MeV^{-1} (consistent with what is known from evaporation spectra), and the average effective mean square matrix element for the residual interactions responsible for energy equilibration. The latter has the empirical form

$$M^2_{jk}=K_{jk}A^{-3}\left(\frac{E}{3}+20.9\ \text{MeV}\right)^{-3}, \tag{6}$$

where j and k give the nature (proton or neutron) of the interacting particles and E is the excitation energy of the composite nucleus. The K_{jk} were determined in Ref. [8] to be $K_{\pi\pi}=5.7\times 10^6$ MeV^5 and $K_{\pi\pi}:K_{\pi\nu}:K_{\nu\nu}=5.7{:}3.4{:}3.4$. Their size is strongly coupled to the size of $g_{\pi 0}$ and $g_{\nu 0}$.

In the equilibrium calculations, a simple Weisskopf-Ewing formula uses Fermi gas model state densities which have been corrected for pairing and shell structure [9] effects based on the pairing energies and shell gaps from the preequilibrium calculations. Emission of a second particle from either the preequilibrium or equilibrium phase of the reaction is allowed, and an approximate method is used to account for the competition of gamma-ray emission with secondary evaporation [9]. The values of the total reaction cross sections in both the entrance and exit channels are a parametrization of the optical model reaction cross sections of Becchetti-Greenlees [30] for protons and Mani *et al.* [31] for neutrons. These have been modified to go over to a geometric cross section at higher energies and to agree with experimental nonelastic cross sections as described in Ref. [8]. In addition, the sub-barrier behavior for protons was empirically altered as discussed in Ref. [9].

B. Results of comparisons

Comparisons of model calculations with experimental spectra from the literature [18–20,25,28,29,32–57] are shown in Figs. 6–14. Only the inelastic scattering results have changed noticeably from Sect. III with the inclusion of the giant resonance states.

For neutron induced reactions, the energy spectra in both the inelastic and exchange channels are now generally well accounted for. The earlier difficulty of underestimating the

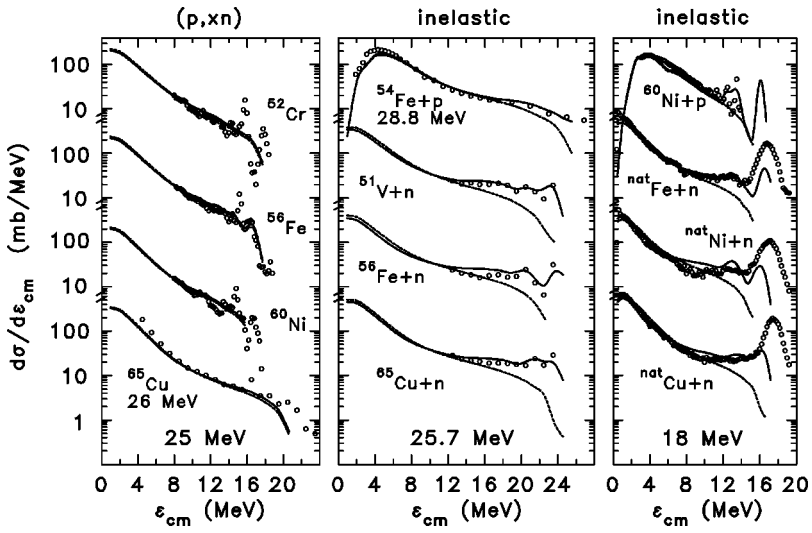

FIG. 8. Comparison between calculation and experiment for reactions on targets with $A=45-65$ at incident energies of 18–26 MeV. The points and curves have the same significance as in Fig. 6. The data are from Refs. [33,37–41].

preequilibrium inelastic scattering at higher emission energies is largely resolved, though a small effect remains for the heavy deformed targets. Both the increased surface localization of the initial interaction and (to a lesser extent) the inclusion of the GR states play a role in improving the overall trend, while the inclusion of the spectroscopic collective states makes the calculations more realistic by accounting for the strong peaks in the spectra. Significantly, the increased surface localization also generally helps the agreement for the (n,xp) spectra.

For proton induced reactions, the changes in the calculated results compared to earlier papers are smaller because there is less difference in the amount of surface localization. The (p,xp) results are, on average, improved by the inclusion of giant resonance collective states.

With regard to the collective state model, there seems to be a general trend for the calculated cross section in the region of the collective states to be underestimated at incident energies above 25 MeV. This suggests that the energy dependence of the model may need to be revised in future work.

Finally, the generally good agreement shown in Figs. 6–14 and the relatively minor role played by the GR states imply that including giant resonance excitations in the model before the study of surface effects would not have significantly altered the results of that study.

VI. SUMMARY AND CONCLUSIONS

Earlier exciton model calculations encountered difficulties in reproducing the relative intensities in the four (N,xN) reaction channels using a consistent set of model input. This paper has shown that different amounts of surface localization of the initial target-projectile interaction for proton and neutron projectiles can explain and remove the problem. The data can be described by $V_{\mathrm{eff},p}=17$ MeV for incident protons

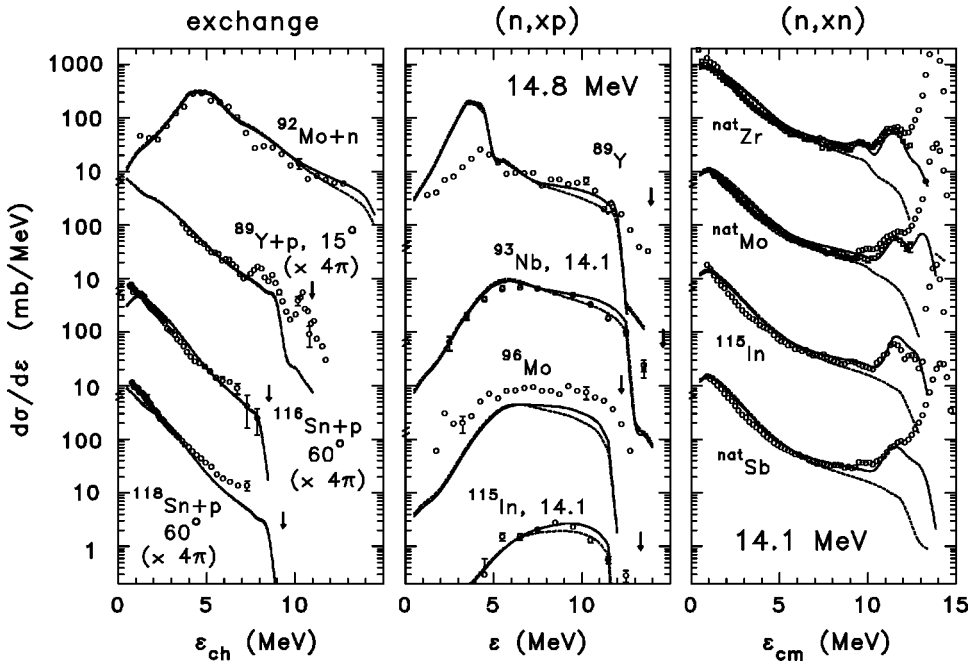

FIG. 9. Comparison between calculation and experiment for reactions on targets with $A=89-125$ at incident energies of 14–15 MeV. The points and curves have the same significance as in Fig. 6. The vertical arrows show the position of the ground state transitions for the exchange reactions. In the left panel, the incident energy for the first two spectra is 14.8 MeV and for the last two it is 14 MeV. The data are from Refs. [19,25,28,42–46].

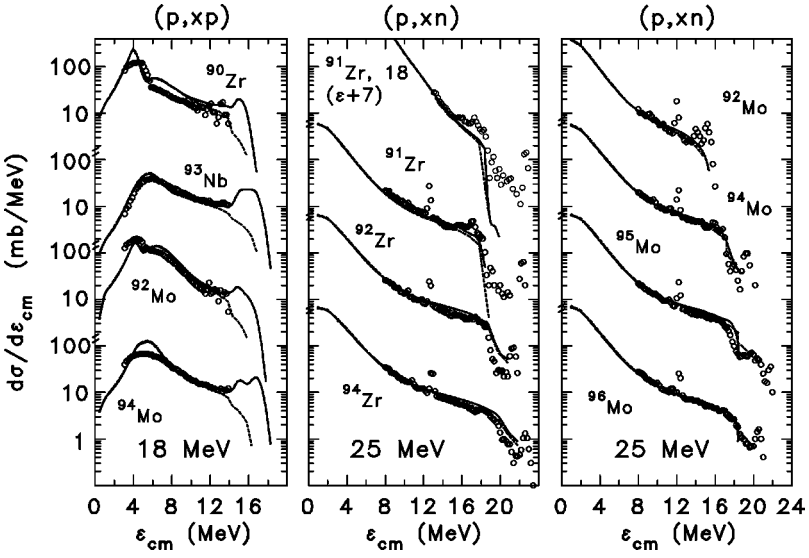

FIG. 10. Comparison between calculation and experiment for reactions on targets with $A = 89-100$ at incident energies of 18 and 25 MeV. The points and curves have the same significance as in Fig. 6, and the data are from Refs. [39,47,48]. The ^{91}Zr(p,xn) results at 18 MeV have been shifted to the right by 7 MeV for display purposes.

at energies up to 100 MeV, while for neutrons the value is smaller, $V_{\mathrm{eff},n} = 7$ MeV, for incident energies up to 26 MeV, thus indicating more surface localization. The only neutron induced reaction to be analyzed at higher energies (60 MeV) suggested a V_{eff} closer to the proton value, but many additional data are needed for neutron reactions above 26 MeV.

To aid in studying surface effects, the excitation of collective states was added to the calculations using the simple model of Ref. [11]. First spectroscopic states representing $2+$, $3-$, and often $4+$ excitations were included since these are prominent features in the energy spectra from inelastic scattering. Later the excitation of isoscalar giant resonance states was added using the same basic model. A table of input parameters for the spectroscopic states for a wide variety of targets is given, and a systematic set of parameters for the GR states is proposed.

With the inclusion of the collective states and the use of different V_{eff} values for proton and neutron projectiles, the exciton model as expressed in the TUNL computer code PRECO is able to successfully account for the full set of about 160 energy spectra from the literature that was used in earlier work. These cover incident energies mainly up to about 29 MeV, with a few reactions at 90 MeV. Additional spectra at energies of 35–100 MeV are also reasonably well described with the same global input set. This represents a major achievement for any preequilibrium model, particularly one as simple and phenomenological as the exciton model.

A further observation from this work is the need for additional continuum energy spectra to be measured. Development and benchmarking of preequilibrium reaction models is dependent on the availability of a wide variety of data. Existing data for (N,xN) reactions are far from uniformly distributed over target mass, incident energy, and reaction type.

The most acute data need is for neutron induced reactions at energies above 26 MeV, both inelastic and exchange, but there is also a lack of (n,xp) spectra at 18 to 26 MeV. Recently results on (n,xp) reactions at incident energies up to 60 MeV measured at the LANSCE facility have begun to appear [58], and this program should provide an excellent

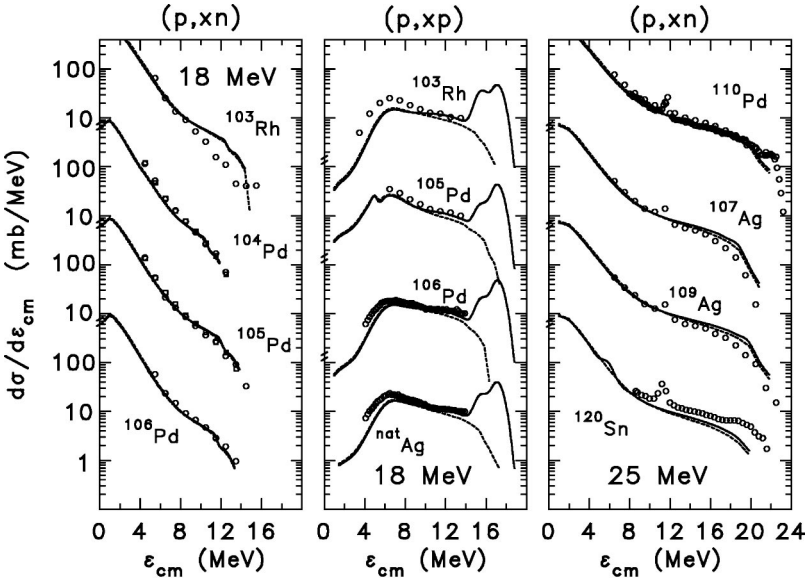

FIG. 11. Comparison between calculation and experiment for reactions on targets with $A = 100-125$ at incident energies of 18 and 25 MeV. The curves and points have the same significance as in Fig. 6, and the data are from Refs. [20,39,48–50].

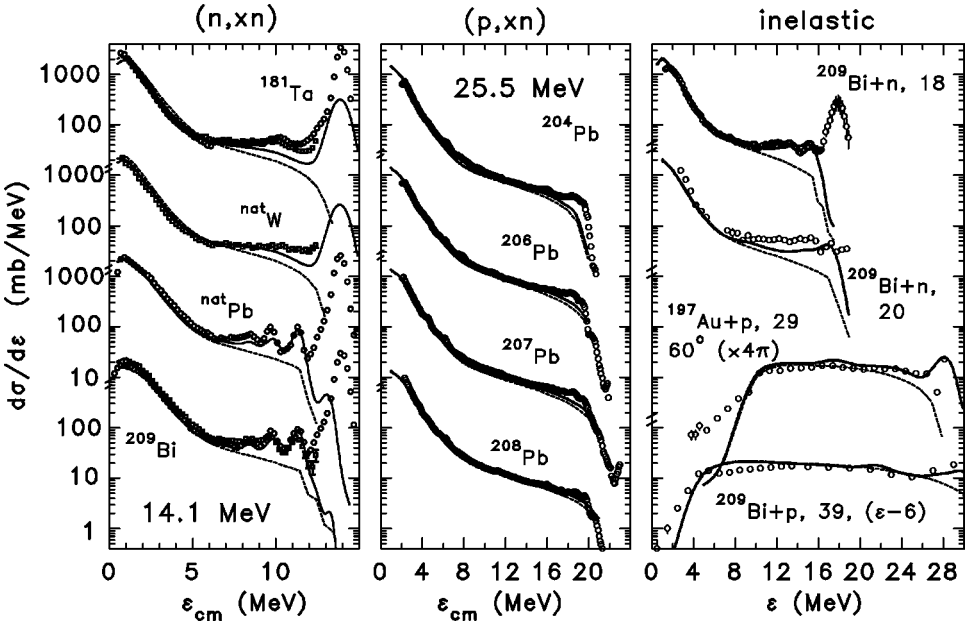

FIG. 12. Comparison between calculation and experiment for reactions on heavy targets at energies of 14–39 MeV. The points and curves have the same significance as in Fig. 6, and the data are from Refs. [18,19,28,37,51,52]. For the inelastic reactions, the projectile energies are shown next to the reaction designations. The ^{209}Bi(p,xp) results are shifted left by 6 MeV for display purposes.

and important source of such data as additional targets are studied. Confirming measurements from another laboratory would also be desirable, along with inelastic neutron scattering measurements above 26 MeV.

Data on proton reactions are more numerous but spotty. There are few measurements at 14 MeV, the (p,xn) are sparse at 18 MeV, while the (p,xp) are somewhat sparse at 25 MeV. At higher energies, inelastic spectra are especially lacking at 80–100 MeV while the 60 MeV spectra are more than 30 years old with frequent evidence of background from the passive collimators often used. Exchange spectra are almost nonexistent at these energies.

With a version of the exciton model giving a robust description of (N,xN) reactions up to at least 30 MeV, attention will be shifted to higher energies where open questions remain. One is the extent of isospin conservation in the preequilibrium phase of the reaction. There is evidence that it is fully conserved at energies up to 25 MeV and preliminary evidence that it is mixed at 90 MeV. If the latter is verified, the question of where and how the transition from conservation to mixing occurs will be addressed. The exciton model parameter for which there is the least *a priori* guidance is the effective matrix element for the residual two body interactions, and its formulation at higher energies needs to be studied. The question of the surface effects for incident neutrons above 26 MeV must still be resolved once data become available in the literature, and the question of the energy dependence of the collective excitation model should be pursued.

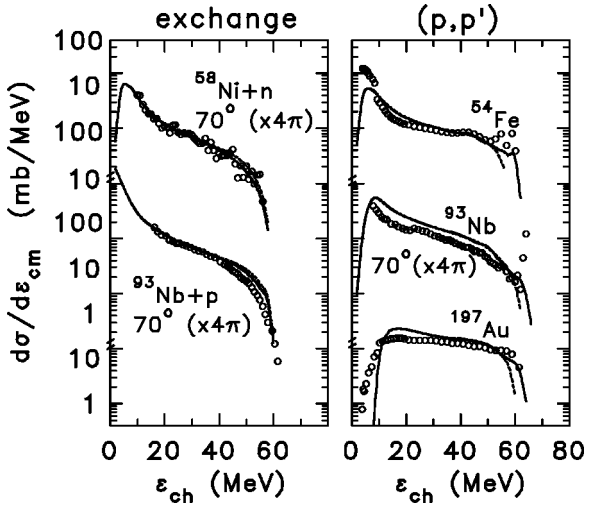

FIG. 13. Comparison between calculation and experiment for reactions at incident energies of 60–65 MeV. The points and solid curves have the same significance as in Fig. 6, and the data are from Refs. [37,53–55]. The dashed curves are new calculations done with the model and input set of Ref. [9].

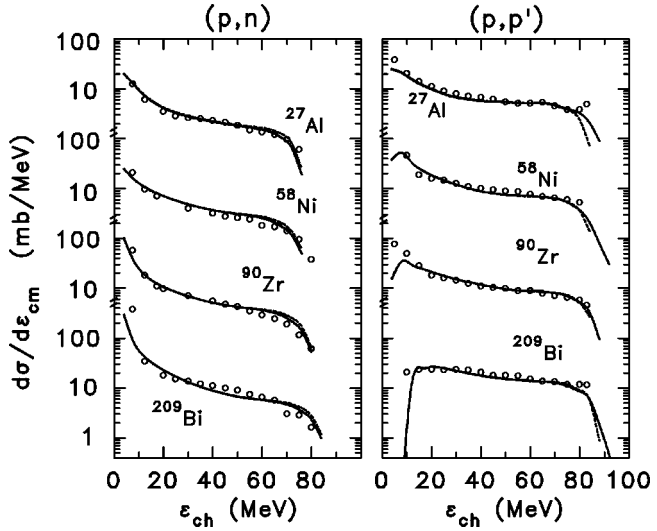

FIG. 14. Comparison between calculation and experiment for reactions at 90 MeV. The points and curves have the same significance as in Fig. 6. The data are from Refs. [56,57].

ACKNOWLEDGMENTS

This work was performed at the Triangle Universities Nuclear Laboratory under U.S. Department of Energy Grant No. DE-FG02-97ER41033. The author would like to thank F. E. Bertrand for helpful comments on giant resonance states and also the various experimentalists who provided their data in tabular form.

[1] J. J. Griffin, Phys. Rev. Lett. **17**, 478 (1966).
[2] M. Blann and H. K. Vonach, Phys. Rev. C **28**, 1475 (1983).
[3] H. Feshbach, A. Kerman, and S. Koonin, Ann. Phys. (N.Y.) **125**, 429 (1980).
[4] Y. Watanabe, A. Aoto, H. Kashimoto, S. Chiba, T. Fukahori, K. Hasegawa, M. Mizumoto, S. Meigo, M. Sugimoto, Y. Yamanouti, N. Koori, M. B. Chadwick, and P. E. Hodgson, Phys. Rev. C **51**, 1891 (1995).
[5] P. Demetriou, A. Marcinkowski, and P. E. Hodgson, Nucl. Phys. **A596**, 67 (1996).
[6] C. Kalbach, J. Phys. G **21**, 1519 (1995).
[7] C. Kalbach, Acta Phys. Slov. **45**, 685 (1995).
[8] C. Kalbach, J. Phys. G **24**, 847 (1998).
[9] C. Kalbach, J. Phys. G **25**, 75 (1999).
[10] C. Kalbach, Phys. Rev. C **32**, 1157 (1985).
[11] H. Kalka, M. Torjman, and D. Seeliger, Phys. Rev. C **40**, 1619 (1989).
[12] C. Kalbach, ''PRECO-E: The Two-Component Exciton Model Code with Direct Reactions and Angular Distributions,'' Los Alamos National Laboratory Report No. LA-UR-91-2300, 1991 (unpublished).
[13] C. Kalbach, Nucl. Sci. Eng. **115**, 43 (1993).
[14] H. Kalka, D. Seeliger, and F. A. Zhivopistsev, Z. Phys. A **329**, 331 (1988).
[15] S. Raman, C. H. Malarkey, W. T. Milner, C. W. Nestor, and P. H. Stelson, At. Data Nucl. Data Tables **36**, 1 (1987).
[16] R. H. Spear, At. Data Nucl. Data Tables **42**, 55 (1989).
[17] R. B. Firestone, V. S. Shirley, C. M. Baglin, S. Y. F. Chu, and J. Zipkin, *Table of Isotopes*, 8th ed. (Wiley, New York, 1996).
[18] A. Takahashi, E. Ichimura, Y. Sasaki, and H. Sugimoto, Osaka University OKTAVIAN Report No. A-87-03 (1987).
[19] A. Takahashi, M. Gotoh, Y. Sasaki, and H. Sugimoto, Osaka University OKTAVIAN Report No. A-92-01 (1992).
[20] C. Kalbach, I. D. Proctor, and D. Heikkinen, unpublished (p,xp) spectra at 25 MeV [see Bull. Am. Phys. Soc. Series II **21**, 663 (1976)]; angle integrated spectra obtained from backward hemisphere data as described in Ref. [6].
[21] Y. Watanbe, T. Kuwata, Sun Weili, M. Higashi, H. Shinohara, M. Kohno, K. Ogata, and M. Kawai, Phys. Rev. C **59**, 2136 (1999).
[22] M. Avrigeanu, A. Harangozo, V. Avrigeanu, and A. N. Antonov, Phys. Rev. C **54**, 2538 (1996).
[23] F. E. Bertrand, Nucl. Phys. **A354**, 129c (1981).
[24] A. van der Woude, in *Electric and Magnetic Giant Resonances in Nuclei*, edited by J. Speth (World Scientific, Singapore, 1991), pp. 99–232.
[25] Y. Watanabe, I. Kumabe, M. Hyakutake, A. Takahashi, H. Sugimoto, E. Ichimura, and Y. Sasaki, Phys. Rev. C **37**, 963 (1988).
[26] A. Marcinkowski, B. Marianski, P. Demetriou, and P. E. Hodgson, Phys. Rev. C **52**, 2021 (1995).
[27] G. R. Satchler, *Direct Nuclear Reactions* (Clarendon, Oxford and Oxford University Press, New York, 1983), p. 601.
[28] M. Baba, S. Matsuyama, T. Ito, T. Ohkubo, and N. Hirakawa, J. Nucl. Sci. Technol. **31**, 757 (1994), and data tables supplied by the authors.
[29] A. Marcinkowski, R. W. Finlay, J. Rapaport, P. E. Hodgson, and M. B. Chadwick, Nucl. Phys. **A501**, 1 (1989).
[30] F. D. Becchetti, Jr. and G. W. Greenlees, Phys. Rev. **182**, 1190 (1969).
[31] G. S. Mani, M. A. Melkanoff, and I. Iori, Centre d'Etudes Nucléaire de Saclay Report No. CEA 2380 (1963).
[32] S. M. Grimes, R. C. Haight, and J. D. Anderson, Nucl. Sci. Eng. **62**, 187 (1977).
[33] Unpublished data tables supplied by M. Baba of results reported in Proceedings of the International Conference on Nuclear Data for Science and Technology, Mito, Japan, 1988, edited by S. Igarishi, p. 291.
[34] S. M. Grimes, R. C. Haight, and J. D. Anderson, Phys. Rev. C **17**, 508 (1978).
[35] S. M. Grimes, R. C. Haight, K. R. Alvar, H. H. Barschall, and R. R. Borchers, Phys. Rev. C **19**, 2127 (1979).
[36] Data tables supplied by M. Baba of results reported in S. Matsuyama, T. Ito, and M. Baba, Japan Atomic Research Institute Report No. JAERI-M,92-027 (1993).
[37] F. E. Bertrand and R. W. Peele, Phys. Rev. C **8**, 1045 (1973).
[38] W. Scobel, L. F. Hansen, B. A. Pohl, C. Wong, and M. Blann, Z. Phys. A **311**, 323 (1983).
[39] W. Scobel, M. Blann, T. T. Komoto, M. Trabandt, S. M. Grimes, L. F. Hansen, C. Wong, and B. A. Pohl, Phys. Rev. C **30**, 1480 (1984).
[40] A. Marcinkowski, R. W. Finlay, G. Randers-Pehrson, C. E. Brient, and J. E. O'Donnell, Nucl. Phys. **A402**, 220 (1983).
[41] Y. Watanabe, K. Kodaka, Y. Kubo, N. Koori, M. Eriguchi, M. Hanada, and I. Kumabe, Z. Phys. A **336**, 63 (1990).
[42] R. Fischer, M. Uhl, and H. Vonach, Phys. Rev. C **37**, 578 (1988).
[43] R. C. Haight, S. M. Grimes, R. C. Johnson, and H. H. Barschall, Phys. Rev. C **23**, 700 (1981).
[44] G. Traxler, A. Chalupka, R. Fischer, B. Strohmaier, M. Uhl, and H. Vonach, Nucl. Sci. Eng. **90**, 174 (1985).
[45] S. M. Grimes, J. D. Anderson, B. A. Pohl, J. W. McClure, and C. Wong, Phys. Rev. C **4**, 607 (1971).
[46] R. M. Wood, R. R. Borchers, and H. H. Barschall, Nucl. Phys. **71**, 529 (1965).
[47] Y. Watanabe, I. Kumabe, M. Hyakutake, N. Koori, K. Ogawa, K. Orito, K. Akagi, and N. Oda, Phys. Rev. C **36**, 1325 (1987).
[48] M. Blann, R. R. Doering, A. Galonsky, D. M. Patterson, and F. E. Serr, Nucl. Phys. **A257**, 15 (1976).
[49] S. M. Grimes, J. D. Anderson, and C. Wong, Phys. Rev. C **13**, 2224 (1976).

[50] C. Kalbach, S. M. Grimes, and C. Wong, Z. Phys. A **275**, 175 (1975).
[51] K. Harder, A. Kaminsky, E. Mordhorst, W. Scobel, and M. Trabandt, Phys. Rev. C **36**, 834 (1987).
[52] A. Marcinkowski, J. Rapaport, R. Finlay, X. Aslanoglou, and D. Kielan, Nucl. Phys. **A530**, 75 (1991).
[53] C. M. Castaneda, J. L. Ullmann, F. P. Brady, J. L. Romero, N. S. P. King, and M. Blann, Phys. Rev. C **28**, 1493 (1983), and data tables supplied by the authors.
[54] H. Sakai, K. Hatanaka, N. Matsuoka, T. Saito, A. Shimizu, T. Motobayashi, and T. Shibata, Phys. Lett. **133B**, 375 (1983).
[55] H. Sakai, K. Hosono, N. Matsuoka, S. Nagamachi, K. Okada, K. Maeda, and H. Shimizu, Nucl. Phys. **A344**, 41 (1980).
[56] A. M. Kalend, B. D. Anderson, A. R. Baldwin, R. Madey, J. W. Watson, C. C. Chang, H. D. Holmgren, R. W. Koontz, J. R. Wu, and H. Machner, Phys. Rev. C **28**, 105 (1983).
[57] J. R. Wu, C. C. Chang, and H. D. Holmgren, Phys. Rev. C **19**, 698 (1979).
[58] F. B. Bateman, R. C. Haight, M. B. Chadwick, S. M. Sterbenz, S. M. Grimes, and H. Vonach, Phys. Rev. C **60**, 064609 (1999).